A Compressive Sensing Approach to Multistatic Radar Change Imaging

Chris Kreucher and Mike Brennan

***Abstract*— This paper describes a new approach for forming change images from multistatic radar data based on compressive sensing (CS). Broadly speaking, change images are naturally sparse in the raw image domain, which suggests a CS reconstruction method. Recent results show that the sparsity of the estimand dictates the number of samples required for faithful reconstruction, meaning a change image can be formed with far fewer measurements than used for conventional radar imaging. Our application has a small number of antennas arranged around the perimeter of a surveillance region, which provide large angular diversity but very poor angular sampling. Furthermore, due to application constraints, the scene is interrogated with limited frequency diversity. We aim to construct a high-resolution change image from the measurements, which are sub-Nyquist both spatially and in frequency. This paper first develops a radar imaging model in the context of CS, and then shows with collected data that a sparseness model improves image utility over conventional methods in our setting.**

***Index Terms*— Change imaging, compressive sensing (CS), radar, sparse model.**

I. Introduction

CHANGE imaging is the process of forming an image of the changes in a region using data collected before and after an event. It continues to be an area of interest in the remote sensing community, with work on developing improved methods for constructing change images [1] and research into automatically classifying regions based on the structure of the change [2]. Recently studied change imaging modalities include radar [3]–[5], electrooptical [6], and hyperspectral [7].

This paper describes a new approach for constructing high-resolution change images using a multistatic radar array. In our application, the array is undersampled with respect to conventional requirements both spatially and in frequency. Image formation using radar data is conventionally done using backprojection [8] or polar formatting [9], [10]. These general-purpose imaging techniques rely on adequately sampled apertures and frequency and do not exploit expected image sparseness. In contrast, in our setting we have a poorly sampled aperture and a small number of frequency samples, yielding far fewer samples than required for conventional radar imaging. However, the change image setting ensures that the resulting image is sparse. These facts motivate an alternative image formation method that exploits image sparsity.

The field of compressive sensing (CS) has developed a rich set of methods for estimating sparse signals from a small number of measurements [11]. A number of authors [12]–[17] have recently explored some of these techniques for radar imaging. In order to apply CS methods, one must have both a sparse signal and an appropriate sampling method [13], [14]. In [12], a through-the-wall imaging application is studied, assuming that the number of targets in the image is very small to meet the sparsity requirements. Their sampling approach is based on randomly selecting physical positions and frequencies using a stepped-frequency continuous-wave (SFCW) radar. Similarly, [16] applies an SFCW radar in the ground-penetrating radar setting. Zhu and Bamler [13] use a CS approach to tomographic synthetic aperture radar (SAR). They apply CS for estimation because in their application the signal can be described by a few point-like contributions. The work they report uses a Fourier sampling method. In [14], a framework for using CS to focus SAR images is proposed. They appeal to the statistical properties of SAR images as a means of justifying the sparseness assumption.

In contrast to these efforts, we focus on change imaging. In this regime, the sparseness assumption is broadly correct. We use a sampling method based on random Fourier projections, which is known to satisfy the CS requirements and can be implemented using a commercial SFCW radar. This paper presents three main contributions. First, we cast change image estimation as a CS problem. Next, we illustrate with real collected multistatic radar data how the change image formed using CS provides a useful high-resolution image free of the sidelobes present in images formed using conventional backprojection. Finally, we show that the CS change imaging algorithm gracefully degrades as the number of measurements are reduced, by illustrating useful images with 100 times fewer measurements than unknowns.

This paper proceeds as follows. First, Section II describes the collected data and develops a model that relates the data to the unknown changes. Next, in Section III we describe how we use CS to estimate changes from the collected data given in this model. Section IV illustrates the method on a field collect. Finally, Section V concludes this paper.

II. Radar Imaging Model

We wish to construct a change image over a ground region using multistatic radar data collected before and after a change. This section develops a model that relates the collected frequency domain data to the unknown change image.

Manuscript received July 19, 2012; revised January 23, 2013; accepted February 10, 2013. Date of publication March 22, 2013; date of current version December 12, 2013. This work was supported by the Air Force Research Laboratory under Contract FA8650-09-M-1549 and Contract FA8650-10-C-1718.

The authors are with Integrity Applications, Ann Arbor, MI 48108 USA (e-mail: ckreuche@umich.edu; mbrennan@integrity-apps.com).

Color versions of one or more of the figures in this paper are available online at http://ieeexplore.ieee.org.

Digital Object Identifier 10.1109/TGRS.2013.2247408

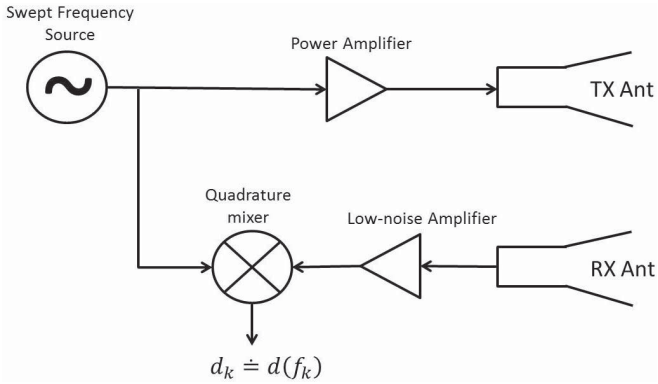

Fig. 1. Nominal SFCW radar.

We assume that the surveillance region is rectangular and characterize a point in the region by its 2-D coordinate (u, v) which is the number of meters east and north, respectively, of a local reference point. The region will be defined by $\{u_{\min}, u_{\max}\}$ and $\{v_{\min}, v_{\max}\}$, and discretized on a regular $N_u \times N_v$ grid with spacing δu and δv (see Table I). Let x denote the $N_u N_v \times 1$ vector of unknowns representing the changes in the $N_u N_v$ pixels, organized u-coordinate major

$$x \leftrightarrow \begin{bmatrix} u_{\min}, v_{\min} \\ u_{\min}, v_{\min} + \delta v \\ \vdots \\ u_{\min}, v_{\max} \\ u_{\min} + \delta u, v_{\min} \\ \vdots \\ u_{\min} + \delta u, v_{\max} \\ \vdots \\ u_{\max}, v_{\max} \end{bmatrix}. \tag{1}$$

Let $\lfloor a \rfloor$ denote the floor of a and $\text{rem}(a, b)$ the remainder when a is divided by b. Then the jth element of x, denoted x_j, corresponds to a cell on the ground centered at

$$\begin{aligned} u_j &= u_{\min} + \delta u \lfloor (j-1)/N_v \rfloor \\ v_j &= v_{\min} + \delta v \, \text{rem}(j-1, N_v). \end{aligned} \tag{2}$$

We take frequency domain radar measurements with a multistatic array before and after a change using an SFCW radar, which measures the scene response at a discrete set of frequencies. It sequentially steps a transmitter through frequency [12] and transmits a gated tone. The signal source dwells at each frequency value long enough to allow echoes from the scene to return to the receiver. The return is then mixed with the transmitted signal, generating a complex-valued measurement which is the response of the scene at that frequency. After stepping through all frequencies, we have the frequency response of the scene at the N_f selected discrete frequencies $f_1, \ldots, f_{N_f}$ [16]. A diagram is shown in Fig. 1.

Let N_p be the number of transmit/receive radar pairs in the array. For convenience, we assume that each pair measures the same bins, although that is not required by the method. We use the complex-valued range-filtered frequency response differences from before and after the change [18] to estimate the change images. The range-filtering step filters out data that would correspond to changes off of the imaging grid.

TABLE I
VARIABLES DESCRIBING THE SURVEILLANCE REGION

Variable	Meaning
u, v	$2D$ Ground location
$u_{\min}, \ldots, v_{\max}$	Spatial extent of u, v grid
N_u, N_v	Number of cells in the u and v directions
$\delta u, \delta v$	Sample spacing in u and v
x	$N_u N_v \times 1$ vector of changes

Formally, the received data at frequency bin k from transmit/receive pair p will be denoted d_k^p, and the change in measurements from before and after a change at frequency bin k from pair p will be denoted Δd_k^p (Table II summarizes this notation). The collection of changes is arranged into an $N_p N_f \times 1$ measurement vector b transmit/receive pair major

$$b = \left[\Delta d_1^1 \cdots \Delta d_k^1 \cdots \Delta d_{N_f}^1 \cdots \Delta d_1^{N_p} \cdots \Delta d_{N_f}^{N_p} \right]^T. \tag{3}$$

The ith element of b corresponds to frequency bin k_i and bistatic transmitter/receiver pair p_i as

$$\begin{aligned} p_i &= 1 + \lfloor (i-1)/N_f \rfloor \\ k_i &= 1 + \text{rem}(i-1, N_f). \end{aligned} \tag{4}$$

p_i corresponds to transmitter T_i and receiver R_i.

We now develop the model of how changes in the surveillance region are reflected in the measurements b. We start by developing a model of how spatial changes map to changes in bistatic range [19], which is the Fourier transform of the measured frequency data. For this purpose, let the vector b^r be the $N_p N_f \times 1$ change in bistatic range measurements which correspond to the $N_p N_f \times 1$ frequency domain measurement vector b. They are related through the $N_p N_f \times N_p N_f$ Fourier matrix F, i.e., $b = F b^r$. Our goal is to develop a linear model $b^r = Ax$ that relates changes in the surveillance region x to changes in bistatic range measurements b^r.

The ith element in b^r corresponds to the range bin

$$\beta_i = 1 + \text{rem}(i-1, N_f). \tag{5}$$

For a target with ranges to the transmitter and receiver r^T and r^R, the bistatic radar range equation [10] says that the power received at the radar, P_r, is related to the transmitted power P_t though the wavelength λ, receiver and transmitter gains G_t and G_r, and target cross section σ as

$$P_r = \frac{P_t G_t G_r \lambda^2 \sigma}{(4\pi)^3 (r^T)^2 (r^R)^2}. \tag{6}$$

Furthermore, the phase of the received signal depends on the total bistatic range and wavelength as $(r^T + r^R)/\lambda$.

For a potential change at physical location (u_j, v_j) as measured by transmitter T_i and receiver R_i with locations (u_{T_i}, v_{T_i}) and (u_{R_i}, v_{R_i}), the ranges are

$$r_{ij}^T = \sqrt{(u_j - u_{T_i})^2 + (v_j - v_{T_i})^2} \tag{7}$$

$$r_{ij}^R = \sqrt{(u_j - u_{R_i})^2 + (v_j - v_{R_i})^2} \tag{8}$$

Fig. 2. Change experiment using a four-element multistatic array (Ant 1–4). Three cylinders (Cyl 1–3) were added and removed from the scene.

TABLE II
VARIABLES DESCRIBING THE RADAR MEASUREMENTS

Variable	Meaning
N_p, p	The number of transmit/receive pairs and a specific pair
N_f, k	The number of measured frequency bins and a specific bin
d_k^p	A measurement from pair p in bin k
Δd_k^p	The difference in d_k^p from before and after a change
b	The $N_pN_f \times 1$ vector of Δd_k^p
F	The $N_pN_f \times N_pN_f$ Fourier Matrix
b^r	The range pseudo-measurements corresponding to b
r_{ij}	The bistatic range from scene pixel j to pair i
Γ_{ij}	The range bin corresponding to r_{ij}
β_i	The range bin for measurement i
A_{ij}	The response from scene pixel j to pair i

and the total bistatic range is $r_{ij} = r_{ij}^T + r_{ij}^R$. This bistatic range r_{ij} corresponds to range bin $\Gamma_{ij} = 1 + \lfloor \text{rem}(r_{ij}, r_{\text{amb}})/\delta_r \rfloor$, where δ_r is the range bin spacing given by the speed of transmission and radar bandwidth ($\delta_r = c/BW$), and r_{amb} is the maximum unambiguous range, given by the bandwidth and the frequency step ($r_{\text{amb}} = BW/\Delta f$).

We can now precisely define the response matrix A, the $N_pN_f \times N_uN_v$ matrix that maps changes at (u_j, v_j) locations to changes in bistatic range measurements. For test cell j and transmitter/receiver pair p_i, the elements of A, A_{ij}, reflect the gain and phase due to the bistatic range from the test cell to the pair. A has nonzero elements only when the spatial location defined by j maps to the bistatic range bin and transmitter/receiver pair defined by i, i.e., where $\Gamma_{ij} = \beta_i$. Let r_i^0 denote the range to scene center for a transmit/receive pair indicated by i. Then the elements of A are

$$A_{ij} = \begin{cases} G_{ij} \dfrac{e^{-\sqrt{-1}4\pi f(r_{ij} - r_i^0)/c}}{r_{ij}^T r_{ij}^R}, & \text{if } \Gamma_{ij} = \beta_i \\ 0, & \text{otherwise.} \end{cases} \tag{9}$$

G_{ij} captures antenna gains, transmit power, and other constants, and is set using calibration collects. In general, (u_j, v_j) will not correspond precisely to a range bin center, and so its energy will spread among neighboring bins. This is approximated in our model by using

$$A_{ij} = \begin{cases} \alpha_{ij} G_{ij} \dfrac{e^{-\sqrt{-1}4\pi f(r_{ij} - r_i^0)/c}}{r_{ij}^T r_{ij}^R}, & |\Gamma_{ij} - \beta_i| < M \\ 0, & \text{otherwise} \end{cases} \tag{10}$$

where M defines the number of neighboring pixels, and α_{ij} is a weight giving the fraction of the energy that a scatterer at (u_j, v_j) puts into the bistatic range bin Γ_{ij}.

With this as background, the model that specifies the relationship between the change image x and the frequency-domain measurements b in the noise-free case is

$$b = \text{FA}x \doteq \Phi x. \tag{11}$$

Φ will be referred to as the sensing matrix, and is $N_pN_f \times N_uN_v$. In practice, the relationship will not be met with equality because of noise.

III. CS FOR CHANGE IMAGE ESTIMATION

Eq. (11) describes how measurements b couple to the unknown change image. In practice, $N_pN_f \ll N_uN_v$, meaning there are fewer measurements than needed to uniquely define the change image. Furthermore, in our experiments, we select to measure only a subset $J < N_pN_f$ projections of the signal. Qualitatively, this means (11) is an underdetermined linear system, meaning many x will explain the measurements b. However, because of the change image setting, we expect x to be sparse. These facts motivate a CS reconstruction method that explits sparseness.

In order to use CS to reconstruct a signal, the signal of interest must be sparse in some basis, and the sensing matrix Φ and the signal sparsifying basis must be mutually incoherent [11], [12]. Since by design our signal, i.e., the change image, is sparse in the image domain, our sparsifying matrix is simply the identity. One sensing matrix that is known to meet the incoherence requirement with an identity sparsifying matrix is a sensing matrix constructed of randomly selected Fourier samples [13], [20]. The sensing matrix Φ in (11) represents a Fourier sampling of the signal.

We use a basis pursuit denoising (BPDN) framework [21], which has been shown to have desirable properties over other related approaches such as matching pursuit in applications like ours [25]. Let ϵ specify an allowable residual error between the projection of the estimate and the measurements. Then BPDN will recover the sparse x from the data b [20] under the conditions described above. That is, solving

$$\min_x ||x||_1 \text{ subject to } ||\Phi x - b||_2 \leq \epsilon \tag{12}$$

generates an estimate of the change image x.

IV. EXPERIMENT

A. Multistatic SFCW Radar Change Imaging Hardware

Our experiments employ an AKELA AVMU500 A SFCW radar. As alluded to above, an SFCW radar is well suited to

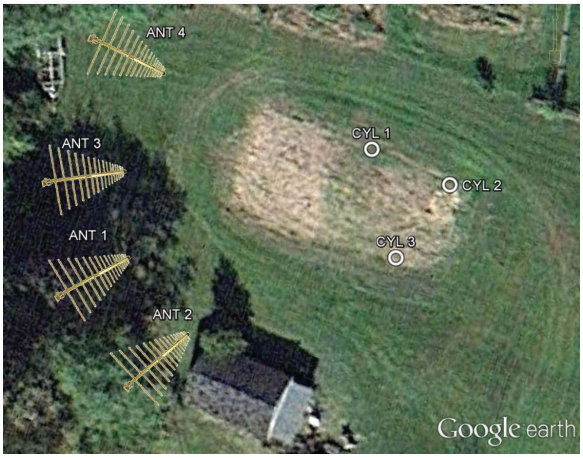

Fig. 3. Surveillance region for the multichange experiment from above (antenna sizes are exaggerated to make them conspicuous).

CS data acquisition because it can be programmed to measure the frequency response at arbitrary frequencies. This usage corresponds to an ability to select rows of the measurement matrix Φ arbitrarily. For the purposes of these experiments, we typically collect measurements at a large number of discrete frequencies and then randomly select which frequencies to use for change image formation in software after the fact. This is logically equivalent to only collecting the random subset of frequencies, but allows us to perform controlled experiments by varying the number of frequency samples used.

The SFCW radar we employ is programmable and capable of transmitting between 300 MHz and 3 GHz. We selected it to sweep through individual frequencies at 45 kHz. By design, the radar steps through the transmit/receive pair because it only has a single transmitter and receiver. This leads to a longer collection time than a more ably equipped unit. However, the objects we are imaging are stationary, and so the speed of data acquisition is not a particularly important factor.

B. Experiment Setup

Our experiment employed the four-element multistatic radar array shown in Fig. 2. The elements in the array are labeled "Ant 1" through "Ant 4." The antenna baseline (measured from Ant 2 to Ant 4) is approximately 25 m, and there is approximately 9 m separating the antennas in the direction perpendicular to the line connecting Ant 2 and 4. The experiment uses cylinders as the changes, which are approximately 1.5 m tall with a 0.2 m diameter. They are located on the order of 35 m away from the array baseline. Fig. 3 shows the layout from above for additional clarity. The antenna locations were measured using a handheld GPS unit operating in differential correction mode. Cylinder locations were measured with a laser range finder.

Data were collected from the six unique bistatic pairs (Tx 1→Rx 2, Tx 1→Rx 3, etc., but not reverse paths) with a center frequency of 2 GHz and bandwidth of 2 GHz. We collected 1500 step frequencies spaced $1.\bar{3}$ MHz apart, giving a total of $6 \times 1500 = 9000$ collected samples. For the purposes of noise reduction, we averaged over several pulses, but there remain only 9000 unique geometry/frequency samples.

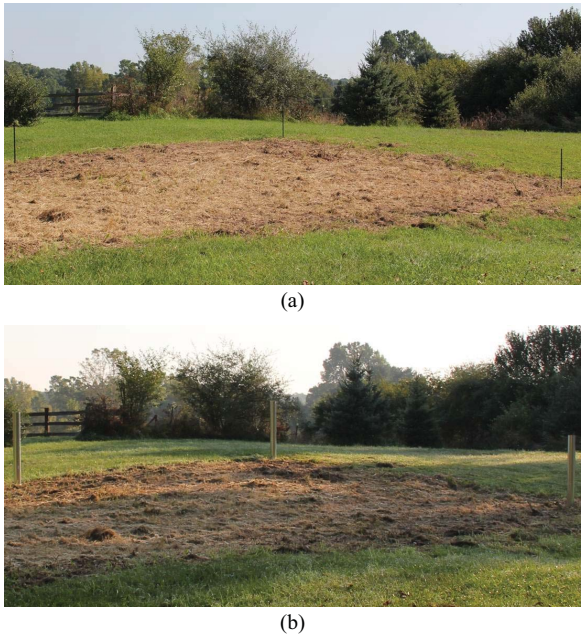

(a)

(b)

Fig. 4. Images from the experiment. (a) Without the cylinders (notice there are support rods which were always present). (b) With the cylinders.

Multistatic echoes were collected before and after the cylinders were placed in the scene. There is a set of support posts underneath the cylinders which remain throughout the experiment. Images showing the scene without the cylinders and after the cylinders were added are given in Fig. 4.

C. Image Formation by CS

The sparse model imaging method presented in Section III was used to form a change image using the data collected before and after the cylinders were placed in the scene. Specifically, (12) was solved as described in [21] and implemented in a publicly available code base called SPGL1. The SPGL1 toolset finds x by solving a sequence of LASSO problems with the required sparsity τ

$$\min_x \|\Phi x - b\|_2 \quad \text{s.t.} \quad \|x\|_1 < \tau \tag{13}$$

via a spectral projected-gradient algorithm. Each solution generates an update to a Newton root-finding algorithm that converges on the location where the residual $\|\Phi x - b\|_2$ is below the noise tolerance ϵ. We chose the noise parameter using a calibration collection where no change occurred. The runtime on a standard Linux computer running MATLAB was on the order of a few minutes.

The imaging region was defined as 40×40 m and discretized into 501×501 cells. This represents 251 001 unknown pixels where we estimate the change. The collected data has just 9000 Fourier projections of this scene.

We also synthetically reduced the number of frequency samples by discarding collected frequency bins. The discarded frequency bins were chosen randomly and were identical in the collections before and after the change. This exactly mimics not collecting those frequency bins in the first place, and allows us to systematically study the breakdown as the number

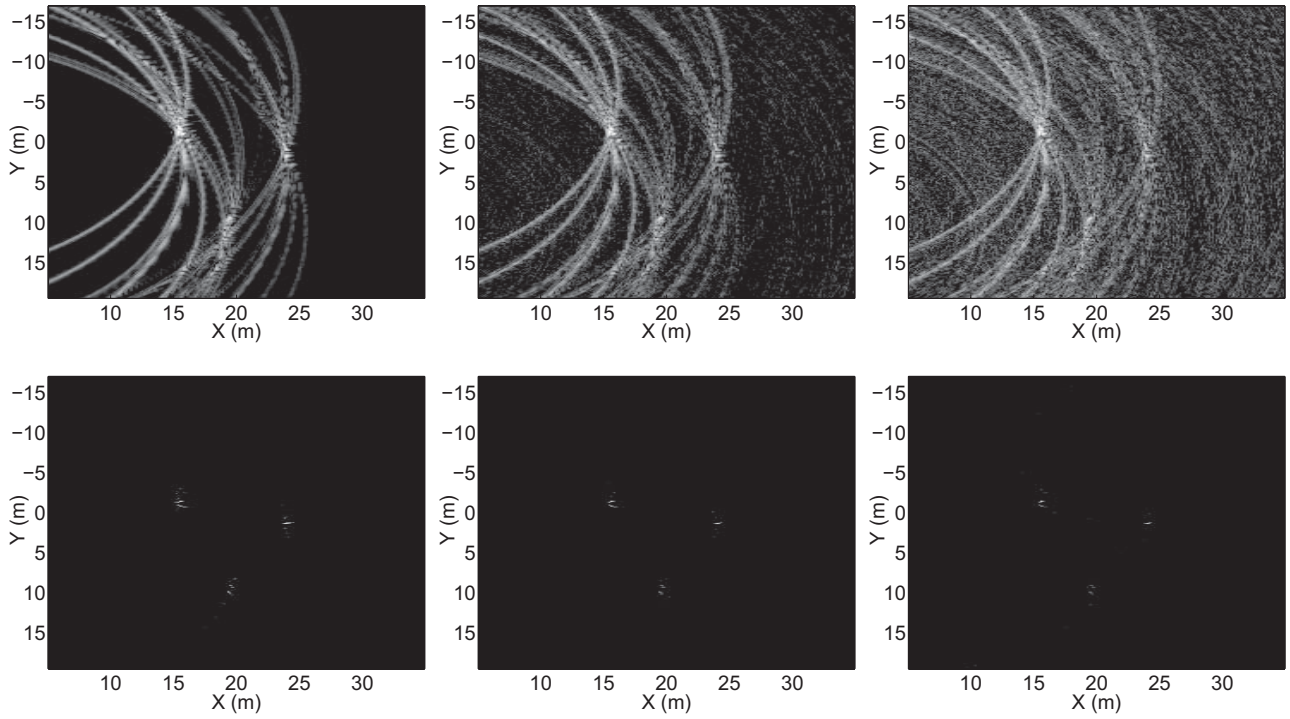

Fig. 5. Backprojection (top) and sparse model (bottom) images with all 9000 collected frequency measurements (left), 40% of the collected measurements randomly discarded (middle), and 70% of the measurements randomly discarded (right). The scales are set to show 20 dB down from the maximum value.

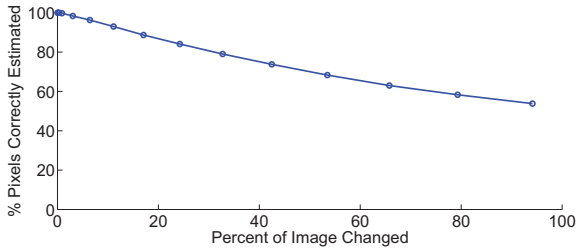

Fig. 6. Algorithm degrading gracefully as the image becomes less sparse.

of measurements is decreased. The results of this experiment are shown in Fig. 5, which includes the image formed using the original 9000 collected samples, and images formed with 40% and 70% of these measurements randomly discarded.

For comparison, we show images formed using backprojection. We used the implementation in [22], which we generalized to the bistatic case, with the same surveillance region and discretization as the CS images. The runtime was less than 1 min. Backprojection is a minimum L_2 solution [23], and can be viewed either in a matched filtering or beamforming context [24]. Qualitatively, it works by mapping each pixel in the surveillance region to each collected range history (which has typically been upsampled). The range entries from multiple pulses (here bistatic pairs) are coherently added to give the value in the image pixel. More discussion on the backprojection technique is given in [8] and [22]–[24].

D. Discussion

The CS change imaging technique localizes all three cylinders well, even when the number of projections is far fewer than the number of unknowns. Cylinder 1 has a stronger return, presumably due to a combination of the bistatic angle and slight material differences. In the case where 9000 frequency domain measurements were used, the relative strength of cylinders 2 and 3 was estimated at 0.7 and 0.5 times that of cylinder 1. In the second case, where 40% of the measurements were discarded, the relative strengths were estimated at 0.64 and 0.35. In the final case where 70% were discarded, the relative strengths were 0.64 and 0.28. All of the cylinder estimates are more than 55 dB above the average background level in the CS images. In comparison, the backprojection image peaks are all less than 15 dB above the background.

E. Performance Versus Sparsity

Our approach exploits the sparsity in the change image. Of interest is the performance when the actual change image is not sparse. We studied this with the following hybrid real data/simulation experiment. First, we characterized the noise by dividing a single real data collect into two sets of pulses, one from early in the collect and one from later. No actual change occurred between the two times, so these frequency differences characterize the noise. Next, we injected synthetic changes (with strength equal to that observed in a real collect) by computing the corresponding frequency differences and adding them to the noise data. We then formed the change image with our CS algorithm, using the same parameters as in Section IV-C. We varied the number of pixels changed and measured the performance by counting the percentage of pixels correctly identified as having changed (or not changed). The results, given in Fig. 6, show that the algorithm degrades slowly as the number of change pixels are increased.

V. Conclusion

We described a new CS approach to forming change images from multistatic radar data. The method generates change images with much more localized energy profiles than conventional backprojection imaging because it exploits the sparsity in the ground plane change image. It is also robust to missing measurements. As alluded to earlier, this comes at the price of increased computations. Furthermore, as the image becomes less sparse, the technique becomes less applicable.

There are several ways this paper could be extended. First, change images could be estimated in three dimensions, avoiding the layover effect present in the current images. Our models generalize straightforwardly, requiring just antenna heights and region elevation to be included in range calculation. Second, the isotropic scattering model ignores angle-dependent changes. It could be modified to include aspect-dependent returns by modifying A, potentially improving image quality. Finally, a study on automated exploitation of the images produced by this algorithm is warranted. The statistics of the CS images are quite different than those of images produced by conventional approaches. As such, current algorithms that exploit these statistics may not be directly applicable.

References

[1] J. Meola, M. Eismann, R. Moses, and J. Ash, "Detecting changes in hyperspectral imagery using a model-based approach," *IEEE Trans. Geosci. Remote Sens.*, vol. 49, no. 7, pp. 2647–2661, Jul. 2011.

[2] S. Martinis, A. Twele, and S. Voigt, "Unsupervised extraction of flood-induced backscatter changes in SAR data using Markov image modeling on irregular graphs," *IEEE Trans. Geosci. Remote Sens.*, vol. 49, no. 1, pp. 251–263, Jan. 2011.

[3] J. Sumantyo, M. Shimada, P. Mathieu, and H. Abidin, "Long-term consecutive DInSAR for volume change estimation of land deformation," *IEEE Trans. Geosci. Remote Sens.*, vol. 50, no. 1, pp. 259–270, Jan. 2012.

[4] H. Wan, "Novel change detection in SAR imagery using local connectivity," *IEEE Geosci. Remote Sens. Lett.*, vol. 10, no. 1, pp. 174–178, Jan. 2013.

[5] J. Zheng and H. You, "A new model-independent method for change detection in multitemporal SAR images based on Radon transform and Jeffrey divergence," *IEEE Geosci. Remote Sens. Lett.*, vol. 10, no. 1, pp. 91–95, Jan. 2013.

[6] X. Sun, W. Chen, R. L. Fischer, M. Jones, J. C. Eichholz, J. E. Richards, P. Shu, M. Jhabvala, A. La, D. Kahle, and J. Adams, "An advanced airborne multisensor imaging system for fast mapping and change detection applications," in *Proc. IEEE Int. Geosci. Remote Sens. Symp.*, Jul. 2007, pp. 600–605.

[7] M. Molinier, J. Laaksonen, and T. Hame, "Detecting man-made structures and changes in satellite imagery with a content-based information retrieval system built on self-organizing maps," *IEEE Trans. Geosci. Remote Sens.*, vol. 45, no. 4, pp. 861–874, Apr. 2007.

[8] D. Munson, J. O'Brien, and W. Jenkins, "A tomographic formulation of spotlight-mode synthetic aperture radar," *Proc. IEEE*, vol. 71, no. 8, pp. 917–925, Aug. 1983.

[9] W. Carrara, R. Goodman, and R. Majewski, *Spotlight Synthetic Aperture Radar*. Norwood, MA, USA: Artech House, 1995.

[10] C. Jakowatz, D. E. Wahl, P. H. Eichel, D. C. Ghiglia, and P. A. Thompson, *Spotlight-Mode Synthetic Aperture Radar: A Signal Processing Approach*. Norwell, MA, USA: Kluwer, 1996.

[11] E. Candes and M. Wakin, "An introduction to compressive sampling," *IEEE Signal Process. Mag.*, vol. 21, no. 2, pp. 21–30, Mar. 2008.

[12] Q. Huang, L. Qu, B. Wu, and G. Fang, "UWB through-wall imaging based on compressed sensing," *IEEE Trans. Geosci. Remote Sens.*, vol. 48, no. 3, pp. 1408–1415, Mar. 2010.

[13] X. Zhu and R. Bamler, "Tomographic SAR inversion by L_1-norm regularization—The compressive sensing approach," *IEEE Trans. Geosci. Remote Sens.*, vol. 48, no. 10, pp. 3839–3846, Oct. 2010.

[14] M. Alonso, P. Lopez-Dekker, and J. Mallorqui, "A novel strategy for radar imaging based on compressive sensing," *IEEE Trans. Geosci. Remote Sens.*, vol. 48, no. 12, pp. 4285–4295, Dec. 2010.

[15] A. Budillon, A. Evangelista, and G. Schirinzi, "Three-dimensional SAR focusing from multipass signals using compressive sampling," *IEEE Trans. Geosci. Remote Sens.*, vol. 49, no. 1, pp. 488–499, Jan. 2011.

[16] A. Gurbuz, J. McClellan, and W. Scott, "A compressive sensing data acquisition and imaging method for stepped frequency GPRs," *IEEE Trans. Geosci. Remote Sens.*, vol. 57, no. 7, pp. 2640–2645, Jul. 2009.

[17] Y.-S. Yoon and M. Amin, "Compressed sensing technique for high-resolution radar imaging," *Proc. SPIE*, vol. 6968, pp. 69681A-1–69681A-10, Mar. 2008.

[18] M. Brennan, C. Kreucher, and B. Shapo, "Multistatic radar change detection using sparse imaging methods," in *Proc. IEEE Workshop Statist. Signal Process.*, Aug. 2012, pp. 532–535.

[19] M. Brennan, C. Kreucher, and B. Shapo, "Multistatic radar change detection using a sparse imaging approach," in *Proc. IEEE Radar Conf.*, May 2012, pp. 45–50.

[20] E. Candes, J. Romberg, and T. Tao, "Stable signal recovery from incomplete and inaccurate measurements," *Commun. Pure Appl. Math.*, vol. 59, no. 8, pp. 1207–1223, Mar. 2006.

[21] E. van den Berg and M. Friedlander, "Probing the Pareto frontier for basis pursuit solutions," *SIAM J. Sci. Comput.*, vol. 31, no. 2, pp. 890–912, Nov. 2008.

[22] L. Gorham and L. Moore, "SAR image formation toolbox for MATLAB," *Proc. SPIE*, vol. 7699, pp. 769906-1–769906-13, Apr. 2010.

[23] F. Natterer, *Mathematics of Computerized Tomography*. New York, USA: Wiley, 1986.

[24] C. Jakowatz, D. Wahl, and D. Yocky, "Beamforming as a foundation for spotlight-mode SAR image formation by backprojection," *Proc. SPIE*, vol. 6970, pp. 69700Q-1–69700Q-15, May 2008.

[25] S. Chen, D. Donoho, and M. Saunders, "Atomic decomposition by basis pursuit," *SIAM J. Sci. Comput.*, vol. 20, no. 1, pp. 33–61, 1998.

Chris Kreucher received the Ph.D. degree in electrical engineering for his dissertation titled "An information-theoretic approach to sensor management" from The University of Michigan, Ann Arbor, MI, USA, in 2005.

He was a member of the research staff in General Dynamics (formerly ERIM) from 1998 to 2007. Since 2008, he has been with Integrity Applications Inc., Ann Arbor, where he is a Principal System Engineer. His current research interests include detection, tracking, multisensor fusion, and sensor scheduling.

Mike Brennan received the M.S. degree (*summa cum laude*) in aerospace engineering from the University of Michigan, Ann Arbor, MI, USA.

He is a Senior Systems Engineer with Integrity Applications Incorporated (IAI). His work includes PM for several radar technology advancement programs and AGI algorithm development for NGA, and he is a Product Chain Analysis Chief Engineer for the Space Radar Program. Prior to IAI, he worked for the General Dynamics Corporation as the Radar Image Chain Analysis Program Manager.